Microstrip ESPAR Antenna With Conical Beam Scanning

Raffaele De Marco, Emilio Arnieri, *Member, IEEE*, Giandomenico Amendola, *Senior Member, IEEE*, and Luigi Boccia, *Senior Member, IEEE*

***Abstract*—This letter introduces a new design for a 2-D electronically steerable parasitic array radiator based on a 3×3 microstrip patch array. The proposed configuration enables conical beam steering by using nine radiating elements, one active U-slot patch antenna, and eight parasitic elements. To validate the proposed design, a prototype was manufactured and experimentally validated. The reported results show a continuous steering range of 75° on the E-plane ($\varphi = 0°$), ranging from $-45°$ to $+30°$, 74° on the H-plane ($\varphi = 90°$) from $-37°$ to $+37°$, and 60° on the D-plane ($\varphi = 51°$), from $-36°$ to $+25°$. The operational bandwidth is about 1.8 %, including the band reduction due to beam scanning. The measured aperture efficiency is equal to 38% with a maximum gain of 8.2 dB.**

***Index Terms*—Beam steering, electronically steerable parasitic array radiator (ESPAR), hybrid antenna, pattern-reconfigurable antennas (PRAs), varactor.**

I. Introduction

PATTERN-reconfigurable antennas (PRAs) offer the ability to electronically direct the beam in a specified direction, making them particularly useful in a rich scattering environment. One of the most promising PRA implementation methods is based on the use of reconfigurable parasitic elements. The two main PRA design approaches are based on parasitic radiators reconfigurable through p-i-n diodes and electronically steerable parasitic array radiators (ESPARs). In both approaches, a single antenna with direct feed is used to excite a set of reconfigurable parasitic elements whose configuration is controlled to direct the beam in a desired direction. Configurations based on p-i-n diodes exploit the concept of the Yagi–Uda antenna where each parasitic element can act as a director or reflector depending on the diodes' configuration [1], [2], [3], [4], [5], [6]. The use of p-i-n diodes implies that there exists a finite number of distinct patterns, which is strongly related to the number of parasitic radiators and to the antenna geometry. An alternative solution that overcomes this limitation is represented by the ESPAR antennas. In this approach, the parasitic elements are loaded with a reactive load, which is used to control the phase of the current, and in turn, the phase of the radiating field. The main advantage of this technique is that the current on the parasitic elements can be modified to achieve a continuous beam steering, miming the operation of phased arrays. In [7] and [8], a 1-D microstrip ESPAR was presented based on a 1×3 lattice.

These solutions allow the beam steering along one plane while having a bandwidth around 1%. To overcome the bandwidth limitations, dielectric resonator antennas (DRAs) were introduced in [9] reaching a fractional bandwidth (FBW) of 4.6%. An alternative approach was employed in [10], which utilizes cavity-backed slot antennas (CBSAs) with coupling irises between the driven antenna and the parasitic radiators. All existing examples of 2-D ESPAR clusters [10], [11], [12], [13] are based on five radiating elements, four of which are parasitically coupled. As shown in [7], this limitation in the number of parasitic radiators is directly linked to the available beam steering directions.

In this letter, a novel design for 2-D beam-scanning microstrip ESPAR antenna is presented. In this arrangement, both the driven and parasitic elements are implemented using standard printed circuit board (PCB) technology, eliminating the need for specialized components to control interelement coupling. This approach allows for a 3×3 configuration, which, when scaled up to larger arrays, enables the use of a regular lattice with one driven element employed every nine array elements. Furthermore, this regular lattice design facilitates scanning in a conical region around boresight. Moreover, the utilization of the conventional PCB technology simplifies the overall configuration of the ESPAR cluster and reduces its manufacturing costs.

II. Antenna Geometry and Operation Principle

The pattern-reconfigurable antenna proposed in this study, as depicted in Fig. 1(a), comprises nine distinct radiators arranged in a 3×3 lattice. Compared to the existing 2-D ESPAR designs, based on a geometry with five elements, in this solution four more parasitic elements that are located along the two diagonal planes are added. This allows the control of the phase gradient along further azimuthal planes, thus, extending the beam scanning capabilities to a conical region. The central element consists of a U-slot patch antenna having width W_D and length L_D. This element serves as a driven element, and it is parasitically coupled with other eight varactor-loaded square patches. The parasitic elements are excited through surface and lateral waves generated by the driven element.

The operational principle is based on the fact that the phase of the surface currents of the parasitic elements can be manipulated by varying the varactor diode junction capacitance [14]. As a consequence, the phase of the radiated field can be controlled implementing the operation principle of the phased array

Manuscript received 4 September 2023; accepted 26 September 2023. Date of publication 29 September 2023; date of current version 5 January 2024. This work was supported by the European Union under the Italian National Recovery and Resilience Plan (NRRP) of NextGenerationEU, partnership on "Telecommunications of the Future" PE00000001 program "RESTART." *(Corresponding author: Raffaele De Marco.)*

The authors are with the Millimeter-Wave Antennas and Integrated Circuit Laboratory (MAIC LAB), University of Calabria, 87036 Quattromiglia, Italy (e-mail: raffaele.demarco@dimes.unical.it; emilio.arnieri@unical.it; g.amendola@dimes.unical.it; luigi.boccia@unical.it).

Digital Object Identifier 10.1109/LAWP.2023.3320790

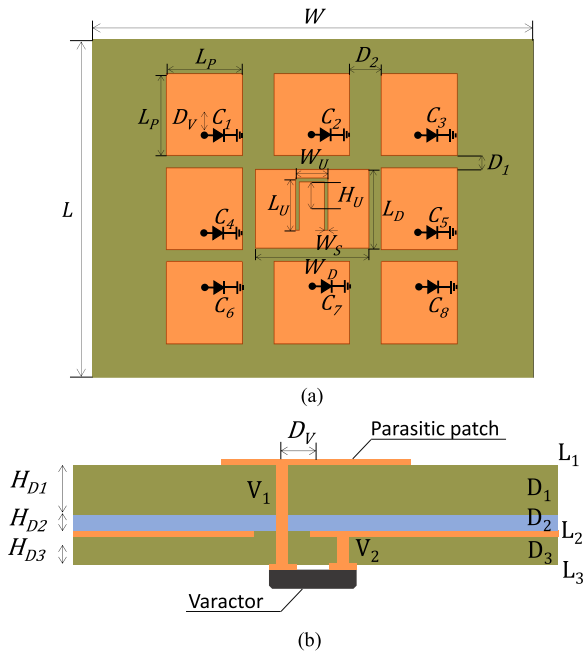

Fig. 1. (a) Antenna geometry. (b) Stack-up (detail of the varactor-loaded parasitic element).

Fig. 2. Equivalent circuit of the varactor diode including the parasitic effects of the package. ($L_{\mathrm{Par}} = 0.4$ nH and $C_{\mathrm{Par}} = 0.06$ pF).

antenna. The key design drivers are related to three components: the driven element, the reactive loaded parasitic element, and the coupling level between the driven and parasitic element. The driven element, which plays a key role in the ESPAR design, must operate over a wide band in order to compensate the alterations of the reflection coefficient due to the change of the parasitic elements' reactive loads. To address this concern, the configuration of the driven element was based on a U-shaped slot antenna, which has been demonstrated to yield significant bandwidth enhancement compared to conventional patch antennas [15]. However, it should be noted that achieving wide bandwidths typically necessitates the use of thicker substrates. In the present case, substrate selection also plays a crucial role as it influences the coupling between the driven and parasitic radiators. Specifically, a thinner substrate facilitates improved coupling on the H-plane [16]. Consequently, a compromise was necessary, balancing the desired bandwidth and the level of coupling between the driven and parasitic elements.

The parasitic elements are implemented through square patches whose side is referred to as L_P. The dimension of the parasitic elements is chosen to have the resonance at 6 GHz when the varactor junction capacitance is settled to the center of the tuning range. In order to control the phase of the field radiated by the parasitic radiators, each element is loaded with a varactor diode. The varactors are connected to the parasitic patches through a via hole, V_1, that goes from the patch, which is printed on the layer L_1 of the stack-up, to the bottom layer of

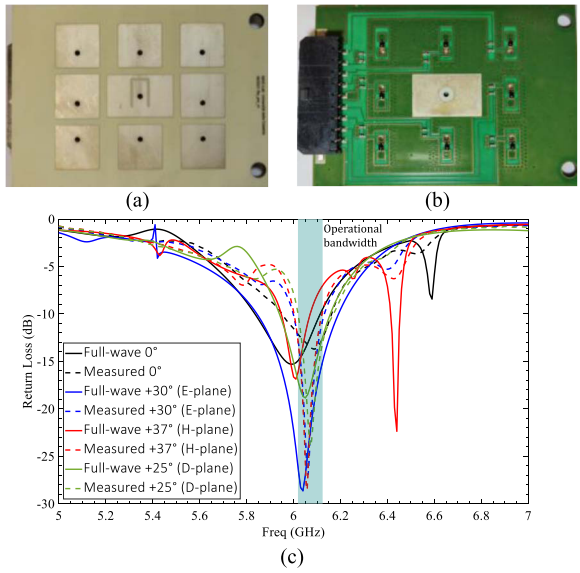

Fig. 3. 3 × 3 ESPAR cluster prototype. (a) Top view. (b) Bottom view. (c) Full-wave and measured return loss for different antenna configurations.

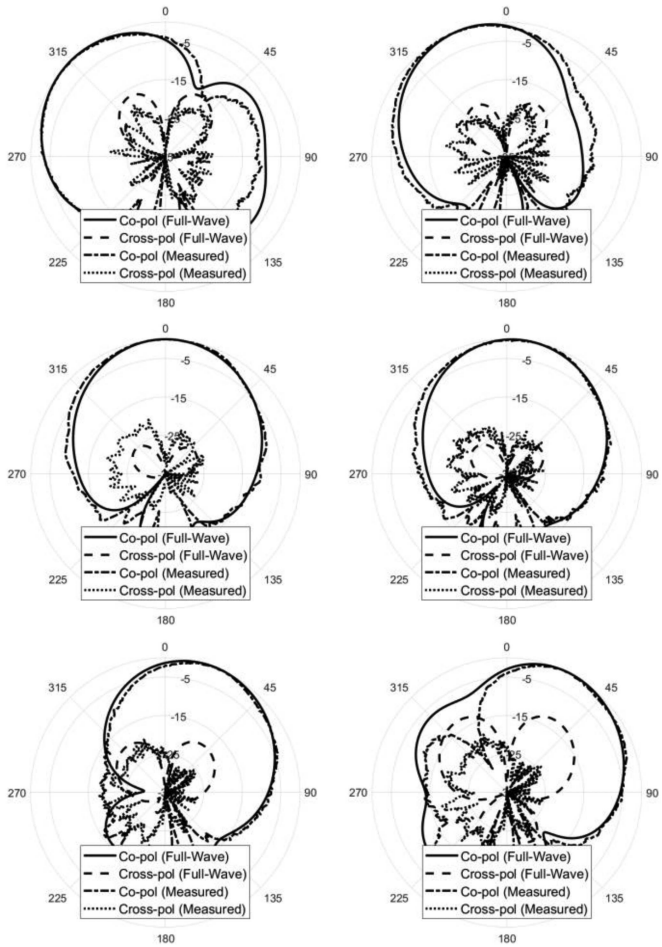

Fig. 4. Full-wave and measured co- and cross-pol E-plane radiation pattern at 6.05 GHz for different antenna configurations.

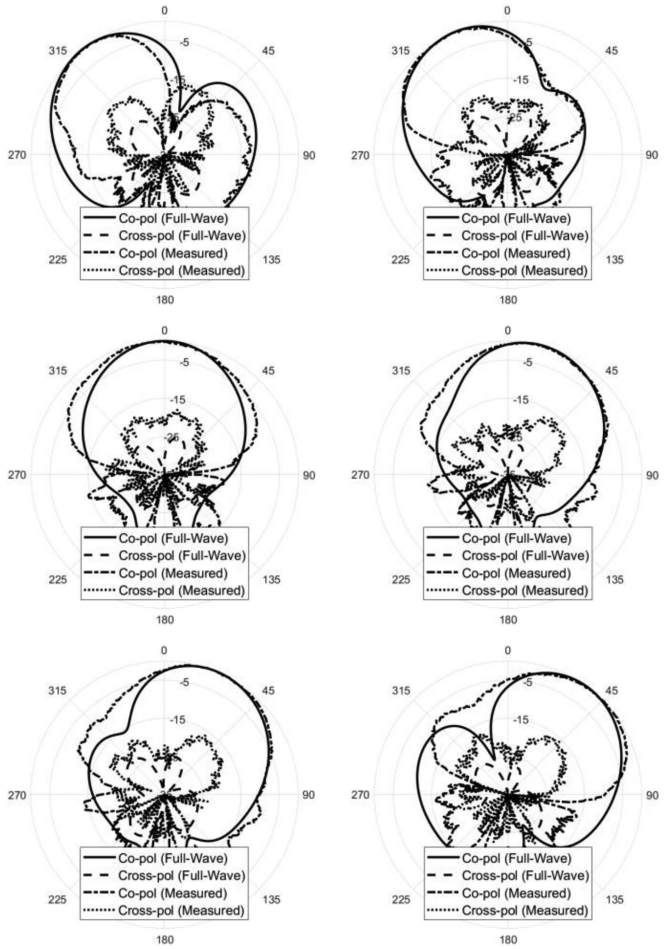

Fig. 5. Full-wave and measured co- and cross-pol H-plane radiation pattern at 6.05 GHz for different antenna configurations.

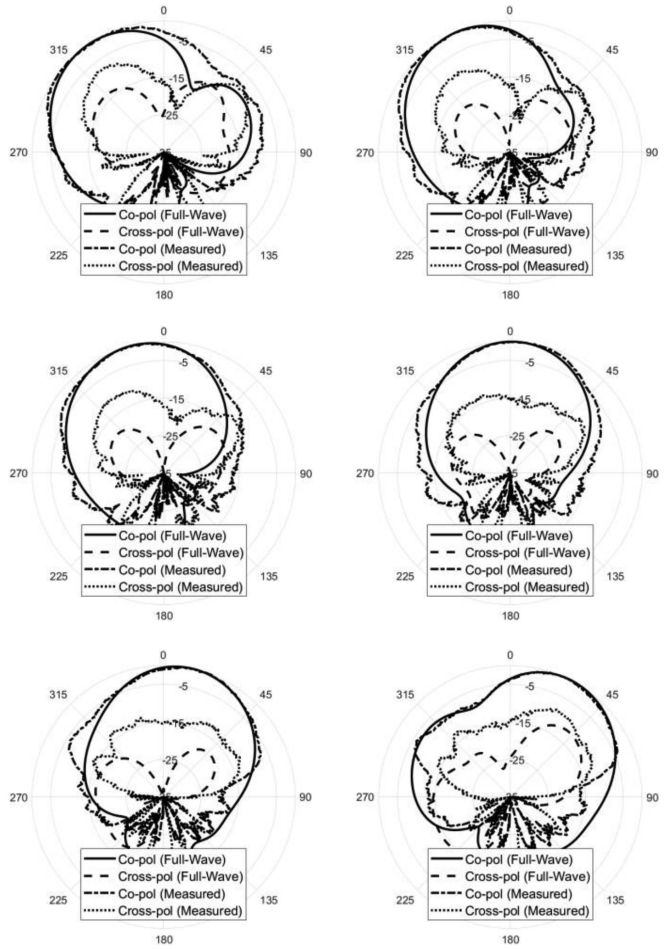

Fig. 6. Full-wave and measured co- and cross-pol D-plane radiation pattern at 6.05 GHz for different antenna configurations.

the PCB, L_3. The position of the via hole, D_V, can be estimated by using the following equation [17]:

$$D_V = \frac{L_P}{\pi}\sin^{-1}\left(\sqrt{\frac{R_i}{R_e}}\right) \tag{1}$$

where R_i is the desired input resistance, 50 Ω, and R_e is the resistance at the edge of the patch. Concerning the coupling level between the driven and parasitic patches, it depends on both the orientation and the distance respect to the driven element [16]. The closer the elements, the larger the current magnitude on the parasitic elements, this results in a wider steering range. On the other hand, a tight coupling affects the input impedance of the driven element causing a degradation of the matching. Therefore, a tradeoff solution must be considered. The antenna stack-up is depicted in Fig. 1(b). It consists of a 1.524 mm thick Rogers RO4350 substrate, D_1, with a relative dielectric constant of 3.66 and a dielectric loss tangent of 0.004. Another Rogers RO4350 dielectric slab, referred to as D_3, having a thickness of 0.254 mm is placed at the bottom side of the PCB to accommodate the varactors and the bias network. A 0.08 mm prepreg layer of Panasonic R-1551, D_2, is used to bond the two dielectric cores.

The actual geometry of the proposed ESPAR cluster was analyzed using a finite-element method (FEM) commercial simulator [18]. A lumped *RLC* model of the varactor was included in the simulation setup. The varactor equivalent circuit, including the packaging effects, is reported in Fig. 2. The diode presents a parasitic inductance L_{par} and a parasitic capacitance denoted as C_{par}. The junction losses are indicated as R_s, whereas the junction capacitance is denoted as C_j, with $j = 1.8$.

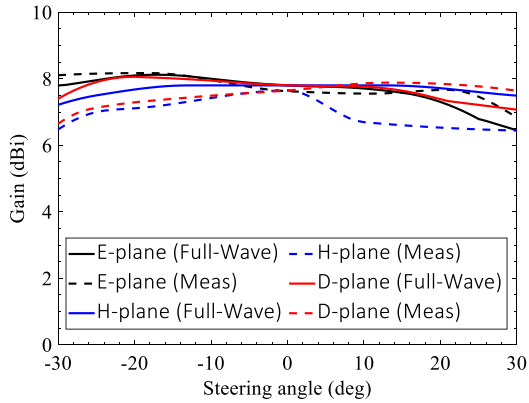

Fig. 7. Full-wave and measured gain at 6.05 GHz versus the steering angle for E-, H-, and D-planes scanning.

To steer the beam to a specific direction, it is essential to determine the appropriate values for varactor junction

TABLE I
KEY GEOMETRICAL PARAMETERS OF THE PROPOSED ANTENNA

Parameter	Value (mm)	Parameter	Value (mm)
L	50	L_U	7.67
W	70	W_U	5.1
H_{D1}	1.524	H_U	3.95
H_{D2}	0.08	D_1	2
H_{D3}	0.254	D_2	5
L_P	12	D_V	2
L_D	11.47	W_S	0.6
W_D	18		

capacitances. In this work, the beam synthesis is obtained by adapting the approach reported in [7] to the specific configuration under investigation. The nine-element ESPAR forms a nine-ports network, where ports from 1 to 8 are terminated with a reactive load $Z_{Cj} = 1/j\omega C_j$. The ratios between the currents on the parasitic patches and the current on the driven element can be derived using network theory as it follows:

$$\begin{bmatrix} \frac{I_1}{I_0} \\ \frac{I_2}{I_0} \\ \vdots \\ \frac{I_8}{I_0} \end{bmatrix} = \begin{bmatrix} Z_{11}+Z_{C1} & Z_{12} & \cdots & Z_{18} \\ Z_{21} & Z_{22}+Z_{C2} & & Z_{28} \\ \vdots & & \ddots & \vdots \\ Z_{81} & & \cdots & Z_{88}+Z_{C8} \end{bmatrix}^{-1} \times x \begin{bmatrix} -Z_{01} \\ -Z_{02} \\ \vdots \\ -Z_{08} \end{bmatrix} \quad (2)$$

where I_0 is the current on the driven element, and Z_{0i} and I_i are the port impedance and the current on the parasitic element ith, respectively. This relation between the parasitic elements' currents is used to create lookup tables, which are in turn employed to obtain the desired pointing direction. The radiation pattern of the cluster can be thus estimated by multiplying the array factor by the element pattern.

III. RESULTS

To validate the proposed design, a prototype was manufactured and experimentally characterized at 6 GHz. Macom MGV125-08 varactor diodes with the package 0805-2 were used to load the parasitic patches. Their junction capacitance ranges from 0.6 to 0.055 pF, when it is reverse biased from 2 to 22 V. All the relevant geometrical parameters' values, obtained through a comprehensive full-wave optimization are documented in Table I. The optimization procedure for the driven element aimed at achieving a 4% bandwidth, without accounting for the bandwidth reduction caused by beam steering. The dimensions of the parasitic elements were determined to achieve a resonance at 6 GHz when the junction capacitance is set to half of the available range.

The full-wave simulated and measured return loss corresponding to scan angles of 0°, +30° in E-plane, +37° in H-plane, and +25° in the D-plane are presented in Fig. 3, along with images of the realized prototype. With respect to simulations, a small upshift is observed. The active impedance variations due to the different beam-steering configurations determines a reduction of the operational bandwidth as it is observed from the reflection coefficient at the driven element, which remains below −10 dB from 6.02 to 6.13 GHz, corresponding to 1.8 % of fractional bandwidth.

TABLE II
COMPARISON OF 2-D BEAM-SCANNING ESPAR ANTENNA

	[10]	[11]	[12]	[13]	This work
Radiating element	CBSA	DRA	DRA	DRA	MPA
Number of radiating elements	5	5	5	5	9
FBW (%)	6.4	< 1	-	3.97	1.8
Phase shifter reduction (%)	80	80	80	80	89
Aperture efficiency (%)	32	58	20.4	15	38
Number of azimuthal scanning planes	4	4	4	4	8
Steer range (deg)	-	86	-	44	75

Figs. 4–6 illustrate various radiation pattern configurations corresponding to the E-, H-, and D-planes, respectively. The comparative analysis between the simulated and measured results demonstrates a notable level of agreement. In particular, for the E-plane, the scanning capability spans approximately 75°, ranging from –45 to +30°. On the H-plane, beam steering is attainable within the range of − 37 to +37°, while on the D-plane, the steering range extends from − 36 to +25 degrees. Due to the symmetry of the array lattice, the results can be extended to the other azimuthal planes. The asymmetry in the steering range on E- and D-plane is due to the uneven coupling levels between the driven element and the parasitic elements along the E-plane, stemming from the inclusion of the U-slot in the driven element. During the scanning process on the E-, H-, and D-plane, the cross polarization levels were found to be below −14, −15, and −10 dB, respectively. Furthermore, the measured sidelobe levels (SLLs) during scanning on the E-, H-, and D-planes were observed to be below −11, −8, and −7 dB, respectively.

The measured antenna gain exhibits a peak value of 8.2 dBi when the beam is steered to −20° on E-plane. A minimum gain of 6.5 dBi is measured when scanning to ±37° on the H-plane. Fig. 7 shows the simulated and measured gain at 6.05 GHz versus the steering angle.

IV. CONCLUSION

In this letter, a new design for the ESPAR antenna was presented. The proposed antenna consists of a 3 × 3 array of microstrip patch antennas allowing conical beam scanning. Compared to other 2-D design examples, reported in Table II, the proposed configuration is the only cluster based on nine radiating cells implemented using simple and low-cost PCB stack-up. At variance of the other techniques, based on DRA or CBA, the operating bandwidth is increased by customizing the design of the driven element which, for the reported example, was implemented using a U-slot patch antenna. This solution led to an operational bandwidth of 1.8% with an aperture efficiency of 38%. The experimental results showed a continuous scanning range of 75° on the E-plane, whereas on the H-plane and D-plane, the scanning capabilities extend approximately to 74° and 60°, respectively.

REFERENCES

[1] M. Jusoh, T. Aboufoul, T. Sabapathy, A. Alomainy, and M. R. Kamarudin, "Pattern-reconfigurable microstrip patch antenna with multidirectional beam for WiMAX application," *IEEE Antennas Wireless Propag. Lett.*, vol. 13, pp. 860–863, 2014, doi: 10.1109/LAWP.2014.2320818.

[2] Y. Yang and X. Zhu, "A wideband reconfigurable antenna with 360° beam steering for 802.11ac WLAN applications," *IEEE Trans. Antennas Propag.*, vol. 66, no. 2, pp. 600–608, Feb. 2018, doi: 10.1109/TAP.2017.2784438.

[3] R. Wang, B.-Z. Wang, G.-F. Gao, X. Ding, and Z.-P. Wang, "Low-profile pattern-reconfigurable vertically polarized endfire antenna with magnetic-current radiators," *IEEE Antennas Wireless Propag. Lett.*, vol. 17, no. 5, pp. 829–832, May 2018, doi: 10.1109/LAWP.2018.2817682.

[4] S.-L. Chen, P.-Y. Qin, W. Lin, and Y. J. Guo, "Pattern-reconfigurable antenna with five switchable beams in elevation plane," *IEEE Antennas Wireless Propag. Lett.*, vol. 17, no. 3, pp. 454–457, Mar. 2018, doi: 10.1109/LAWP.2018.2794990.

[5] L. Xing, J. Zhu, Q. Xu, D. Yan, and Y. Zhao, "A circular beam-steering antenna with parasitic water reflectors," *IEEE Antennas Wireless Propag. Lett.*, vol. 18, no. 10, pp. 2140–2144, Oct. 2019, doi: 10.1109/LAWP.2019.2938872.

[6] H. Liu, S. Gao, and T. H. Loh, "Compact dual-band antenna with electronic beam-steering and beamforming capability," *IEEE Antennas Wireless Propag. Lett.*, vol. 10, pp. 1349–1352, 2011, doi: 10.1109/LAWP.2011.2177059.

[7] Y. Yusuf and X. Gong, "A low-cost patch antenna phased array with analog beam steering using mutual coupling and reactive loading," *IEEE Antennas Wireless Propag. Lett.*, vol. 7, pp. 81–84, 2008, doi: 10.1109/LAWP.2008.916689.

[8] J. J. Luther, S. Ebadi, and X. Gong, "A low-cost 2x2 planar array of three-element microstrip electrically steerable parasitic array radiator (ESPAR) subcells," *IEEE Trans. Microw. Theory Techn.*, vol. 62, no. 10, pp. 2325–2336, 2014, doi: 10.1109/TMTT.2014.2345335.

[9] M. R. Nikkhah, J. Rashed-Mohassel, and A. A. Kishk, "Compact low-cost phased array of dielectric resonator antenna using parasitic elements and capacitor loading," *IEEE Trans. Antennas Propag.*, vol. 61, no. 4, pp. 2318–2321, Apr. 2013, doi: 10.1109/TAP.2012.2237535.

[10] W. Ouyang and X. Gong, "A 20-element cavity-backed slot electronically steerable parasitic array radiator (ESPAR) with 2-D beamsteering and minimized beam squint," *IEEE Antennas Wireless Propag. Lett.*, vol. 19, no. 8, pp. 1420–1424, Aug. 2020, doi: 10.1109/LAWP.2020.3004595.

[11] M. R. Nikkhah, P. Loghmannia, J. Rashed-Mohassel, and A. A. Kishk, "Theory of ESPAR design with their implementation in large arrays," *IEEE Trans. Antennas Propag.*, vol. 62, no. 6, pp. 3359–3364, Jun. 2014, doi: 10.1109/TAP.2014.2309958.

[12] R. Movahedinia, M. R. Chaharmir, A. R. Sebak, M. R. Nikkhah, and A. A. Kishk, "Realization of large dielectric resonator antenna ESPAR," *IEEE Trans. Antennas Propag.*, vol. 65, no. 7, pp. 3744–3749, Jul. 2017, doi: 10.1109/TAP.2017.2705024.

[13] R. Movahedinia, A.-R. Sebak, M. R. Chaharmir, M. R. Nikkhah, and A. A. Kishk, "X-band circularly polarized electronically steerable parasitic array radiator of DRA," *IEEE Trans. Antennas Propag.*, vol. 66, no. 2, pp. 721–728, Feb. 2018, doi: 10.1109/TAP.2017.2780895.

[14] R. De Marco, L. Boccia, E. Arnieri, and G. Amendola, "Phased arrays based on hybrid clusters," in *Proc. Microw. Mediterranean Symp.*, 2022, pp. 1–4, doi: 10.1109/MMS55062.2022.9825606.

[15] K.-F. Lee and T. Huynh, "Single-layer single-patch wideband microstrip antenna," *Electron. Lett.*, vol. 31, no. 16, pp. 1310–1312, 1995, doi: 10.1049/el:19950950.

[16] R. Jedlicka, M. Poe, and K. Carver, "Measured mutual coupling between microstrip antennas," *IEEE Trans. Antennas Propag.*, vol. AP-29, no. 1, pp. 147–149, Jan. 1981, doi: 10.1109/TAP.1981.1142529.

[17] T. A. Milligan, *Modern Antenna Design*, 2nd ed. Hoboken, NJ, USA: Wiley, 2005.

[18] Ansys Electronic Desktop, Release 21.2.

Open Access provided by 'Università della Calabria' within the CRUI CARE Agreement